2024 IEEE International Conference on Robotics and Automation (ICRA 2024)
May 13-17, 2024. Yokohama, Japan

# A Hierarchical Framework for Robot Safety using Whole-body Tactile Sensors

Shuo Jiang and Lawson L.S. Wong

***Abstract*— Using tactile signal is a natural way to perceive potential dangers and safeguard robots. One possible method is to use full-body tactile sensors on the robot and perform safety maneuvers when dangerous stimuli are detected. In this work, we proposed a method based on full-body tactile sensors that operates at three different levels of granularity to ensure that robot interacts with the environment safely. The results showed that our system dramatically reduced the overall collision chance compared with several baselines, and intelligently handled current collisions. Our proposed framework is generalizable to a wide variety of robots, enabling them to predict and avoid dangerous collisions and reactively handle accidental tactile stimuli.**

## I. INTRODUCTION

In recent times, many types of tactile sensing equipment have been designed using different technologies [1], [2], [3], [4], [5], which have been applied to robot tasks such as shape exploration [6], texture recognition [3], [7], physical properties identification [8], [9] or human-robot interaction [10], [11], [5]. Other than perception, the function of safeguarding the robot from dangerous contacts also plays an important role. Oftentimes can a robot be damaged by self-collision or environmental uncertainty, so the goal of *tactile safety* is to avoid or handle dangerous tactile stimuli.

Based on whether a tactile event is predictable, it can be categorized into either static or dynamic [12]. It has been biologically evidenced that animals respond to different types of tactile stimuli with hierarchical engagement of the nervous system [13], [14], [15]. For predictable static stimuli, a model should be learned to predict the outcome of actions-environment interaction to avoid repetitive damage and re-plan motion from the learned model to improve operational safety. For dynamic stimuli, animals generally process them through lower-level nervous system, allowing faster responses. *Tactile defensiveness* is a common animal behavior to retract limbs or body from unexpected tactile stimuli, such as forces, temperature or tactile recognition (consider you touch and recognize a spider in blind box). Such behavior has been widely observed in insects [16], crustaceans [17], [18], amphibians [19], fish [20], and mammals [21], [22]. In humans, flexor reflex circuits [23] are mainly responsible for executing such mechanism and it is fundamental to animals' navigation, foraging, reproduction, social, and defensive behavior and is crucial for their survival.

Analogous to robots, we assume that adopting a hierarchical processing approach for different types of tactile stimuli is a feasible strategy. We proposed a general robot tactile safety framework operating at three levels of hierarchies. At the highest level, the "strategy layer", the robot collects long-term action-contact data and learns a model to predict motion risk. Such model affects future global motion planning that unsafe actions are less likely to be chosen. At the middle level or the "modulation layer", the learned model will locally safeguard the robot by modulating unsafe velocities. Finally the lowest level or the "tactile defensiveness layer" mimics animals' tactile defensiveness behavior by retracting the robot from dangerous contact. We designed independent experiments on the above three layers of safety mechanisms to verify their feasibility on different granularities and different types of robots. On a robot equipped with a modular artificial skin, we demonstrated how our proposed tactile safety system can protect workers in a human-robot collaboration task.

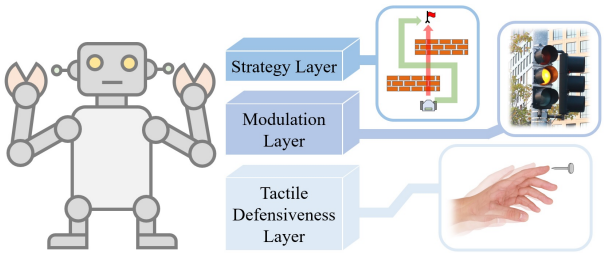


Fig. 1: Three hierarchical layers guarding the robot safety. Strategy layer: model learning and danger-free path planning; Modulation layer: reducing velocity when model indicates danger; Tactile Defensiveness layer: retraction motion under tactile stimulus.

## II. RELATED WORKS

In the past few decades, a variety of robot skins based on different electronic principles have been designed [24] with applications in locomotion [25], human-robot interaction [26], [27], [11], tactile perception [3], [7], etc., however rarely have we seen works discussing robot safety based on on-body tactile sensor array. Many robot systems rely on distant sensors (camera, Lidar) or Force/torque (F/T) sensors to ensure operational safety but they both have limitations. Distant sensors have severe occlusion problem in cluttered scenarios like foliage or terrible sensing condition such as in mud or fog [28]. Joint F/T sensors have ambiguity problem in locating contact position [29] and force distribution [28], which can easily cause unexpected damage [30]. And the control methods based on this type of sensors for safety purpose can be categorized as: passive [31], pre-defined trajectory [32], force control [33], [30], [34], off-line planning [11] and online planning [35], [36]. Previous solutions

This work was supported by NSF Grant #2142519.
Northeastern University, Boston, MA 02115, USA
shuo.jiang@northeastern.edu ; lsw@ccs.neu.edu

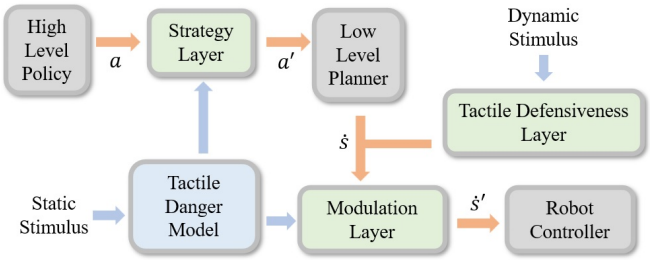


Fig. 2: Block diagram of our tactile safety mechanism.

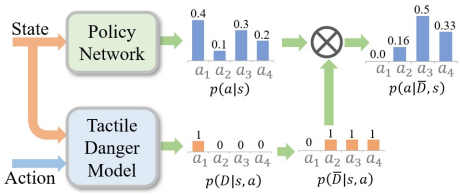


Fig. 3: Tactile danger model pipeline.

only considered mechanical interaction, but little is known for other types of tactile sensing, such like temperature or tactile perception. For example, when you touch a spider and recognize it, how such perception result can be integrated in the controller that retracts your hand is unknown.

Here we briefly summarize some of the previous works on tactile array in the safety context. [28] proposed a model-free approach with high-level model predictive controller and low level impedance controller. The robot is equipped with a capacitive forearm tactile sensor array of 384 taxels. Their experiment showed the robot was able to reach the goal position without causing excessive contact force. Similar system has been designed in [33] with 3,495 taxels and force feedback control. [32] designed an embedded camera-based tactile sensor array mounted on the forearm of a robot. They demonstrated that the robot with such skin retracted from single external poke. [35] designed a serpentine structure deformable robot skin that can be conformally attached to complex surfaces of cobots. When the cobot senses contact, it re-plans its trajectory to avoid it. [25] designed a plantar robot skin on the foothold of a biped robot to achieve walking balance. The robot skin senses the force distribution on the footholds and adjust the robot's walking pattern when it shows unstable. They showed that the F/T sensors failed to detect the unsafe situation and caused the robot to fall. [27] designed a forearm robot skin for nursing robot with arrays of proximity and pressure sensors to perform patient lifting tasks. When an approaching object is detected, the robot reduces its speed and adjusts the patient's position in the arm according to the force distribution. [30] compared different force control methods for an iCub robot with a full-body tactile array. They concluded that accurate contact point estimation is critical for force control tasks. Most of these works are designed for specific application scenarios and robot structures, and hard to be transplanted to different types of robots. Additionally, the obstacle avoidance mechanisms are all model-free, meaning the same dangerous collisions could be revisited.

## III. HIERARCHICAL TACTILE SAFETY

The block diagram of our proposed mechanism is shown in Fig. 2. The three layers can work cooperatively in hierarchy or solely to safeguard robot. Strategy layer relies on tactile danger model (TDM) and Bayes' rule to filter out high-level unsafe actions ($a \to a'$). TDM is trained to predict static contact from state-action pairs. Modulation layer utilizes the learned TDM to perform local velocity modulation ($\dot{s} \to \dot{s}'$), which can either be translated from the planner or from tactile defensiveness layer. The tactile defensiveness layer reactively perceives and handles dynamic stimulus and plans a retraction trajectory.

### A. Strategy Layer

The strategy layer manifests itself through long-term danger-free planning and tactile memory learning. The method employs a neural network to learn tactile memory and uses Bayes' rule to filter out the unsafe actions.

Assuming the tactile sensors are labelled as $i$, we define a binary *single tactile danger event* as sensor $i$ detects danger, $d_i = \mathbb{1}(f_i > f_{th})$, where the stimulus $f_i$ on sensor $i$ exceeds a threshold $f_{th}$. The *total tactile danger event* is the union of all single tactile danger events $D = \bigcup_i d_i \in \{0,1\}$. For each sensor, a tactile danger model is represented by a probability $p(d_i|s,a)$ that a single tactile danger event happens conditioned on robot state $s \in \mathbb{R}^d$ and action $a \in \mathbb{R}^m$ to be taken. Then, the *total tactile danger model* summarizing all sensors can be expressed as:

$$p(D|s,a) = 1 - p(\bar{D}|s,a) = 1 - \prod_i [1 - p(d_i|s,a)] \tag{1}$$

Similarly, we have the total tactile safety model $p(\bar{D}|s,a) = \prod_i [1 - p(d_i|s,a)]$, which is the complement of total tactile danger model. Another important definition we should make here is the *marginal total tactile danger model* $p(D|s)$, which characterizes the probability that the total tactile danger event happens agnostic to action $a$. The model can be learned by importance sampling in a data-driven fashion.

$$\begin{aligned} p(D|s) &= \int p(D|s,a)\, U(a|s)\, da \\ &= \mathbb{E}_{a\sim p(a|s)} \left[ p(D|s,a) \frac{U(a|s)}{p(a|s)} \right] \end{aligned} \tag{2}$$

where $p(a|s)$ is the robot policy. $U(a|s)$ is the homogeneous exploration policy that takes all possible actions with a uniform distribution. Similarly, we can derive marginal total tactile safety model as $p(\bar{D}|s) = 1 - \mathbb{E}_{a\sim p(a|s)} \left[ p(D|s,a) \frac{U(a|s)}{p(a|s)} \right]$. The danger-aware policy incorporating tactile safety model can be derived by Bayes' rule as:

$$\begin{aligned} p(a|\bar{D},s) &= \frac{p(\bar{D}|a,s)\, p(a|s)}{p(\bar{D}|s)} \\ &= \frac{\prod_i [1 - p(d_i|s,a)]\, p(a|s)}{1 - \mathbb{E}_{a\sim p(a|s)} \left[ p(D|s,a) \frac{U(a|s)}{p(a|s)} \right]} \end{aligned} \tag{3}$$

Equation 3 can be regarded as a safeguard to the robot policy. The original policy $p(a|s)$ proposed by robot will be filtered by Equation 3 by incorporating tactile danger model

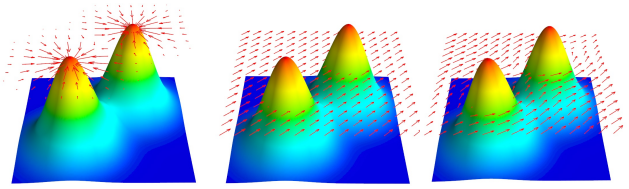

(a) (b) (c)

Fig. 4: (a) Gradient field of the tactile danger potential; (b) example tactile danger potential and the original velocity; (c) modulated velocity avoiding high potential area.

(TDM) proposed in Equation 1 and the marginal model in Equation 2. The new robot policy $p(a|\bar{D},s)$ will be executed by assigning less chance in the direction of tactile danger. A numerical example of the pipeline of the action filtering is shown in Fig. 3. When TDM detects an action $a_1$ is dangerous, it shall reduce the chance that $a_1$ being sampled in the original policy.

### B. Modulation Layer

The modulation layer aims to use the TDM learned in strategy layer to locally regulate the robot velocity. First, we will extend the concept of TDM to a potential field.

*1) Tactile Danger Potential:* In modulation layer, we parameterize TDM in Equation 1 with differentiable parameters $\varphi$, and define the *tactile danger potential* as a mapping from state $s$ and action $a$ to the expectation of danger event $D$:

$$p(D|s,a) \to \mathbb{E}[D] = f_\varphi(s,a) \tag{4}$$

Its normal vector $n(s,a)$ at $s$ and $a$ can be extracted by differentiation (Fig. 4)

$$n(s,a) = \frac{\partial f_\varphi(s,a)}{\partial s} \in \mathbb{R}^d \tag{5}$$

*2) Velocity Modulation:* We extend the modulation strategy in [37] to the context of our tactile danger potential. Assuming the original robot dynamics is modelled as $\dot{s} = g(s,a)$, the modulated dynamics is

$$\dot{s} = \mathbf{M} \cdot g(s,a) \tag{6}$$

with $\mathbf{M} = \mathbf{E} \cdot \mathbf{D} \cdot \mathbf{E}^{-1}$ and

$$\begin{aligned} \mathbf{E} &= [n/|n|, e_2, \cdots, e_d] \\ \mathbf{D} &= diag(\lambda_n, \lambda_2, \cdots \lambda_d) \\ \lambda_n &= 1 - f_\varphi(s,a) \\ \lambda_i &= 1 + f_\varphi(s,a), \quad 2 \le i \le d \end{aligned} \tag{7}$$

Note that the matrices $\mathbf{M}$, $\mathbf{D}$, $\mathbf{E}$ depend on $s$, but not shown explicitly. $n$ is the normal vector defined in Equation 5 and $e_2, \cdots, e_d$ are the bases in the tangential space of $n$. A demonstration of such modulation is shown in Fig. 4. The tactile danger potential penalizes the velocity towards high potential area by reducing the eigenvalue of normal direction $\lambda_n$ and encourage the tangential velocity by amplifying the eigenvalues in the tangential directions $\lambda_i$.

**Theorem 1.** *Modulated dynamics in Equation 6 prevents the robot from initiating tactile danger events with an accurate tactile danger model.*

Fig. 5: (left) TDM learns a sharp edge where the velocity is not penalized until at the boundary; (right) the smoothed model penalizes the velocity before reaching the collision boundary.

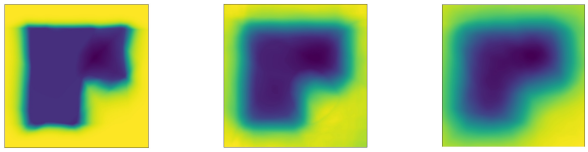

(a) (b) (c)

Fig. 6: (a) original tactile danger potential $f_\varphi$, action has been marginalized for visualization; (b,c) n-step tactile danger potentials $w_\phi(s,a)$ with T=4,8.

Due to the space limit, the proof is not shown here but the idea of proof can be referred to [38] Theorem 2.

*3) N-step Tactile Danger Potential:* A critical issue is that a well-trained TDM may show a sharp edge at the boundary between free space and object surface due to the binary training labels. Thus, velocity will only be modulated in a narrow boundary region, because the step-function-like potential field only has a non-trivial gradient in such region (Fig. 5 left). Instead, to endow robots with the ability to foresee imminent danger (Fig. 5 right), we propose a multi-step tactile potential $w_\phi(s,a)$ to model the expectation of the discounted sum of all future tactile dangers starting from $s$. Such new potential can be estimated by running off-line Monte Carlo in the original tactile danger potential $f_\varphi(\cdot)$.

$$\begin{aligned} w_\phi(s_0,a_0) &= \mathbb{E}_{s_{1:T},a_{1:T}\sim\pi'(s_t)}\left[\sum_{t=0}^{T}\gamma^t \cdot D_t\right] \\ &= \mathbb{E}\left[D_0 \cdot \sum_{t=1}^{T}\gamma^t \cdot D_t \cdot p(D_t|s_t,a_t) \cdot \pi'(a_t|s_t) \cdot p(s_t|s_{t-1},a_{t-1})\right] \end{aligned} \tag{8}$$

$\gamma \in (0,1)$ is a discount factor. $\pi'(s_t)$ can be arbitrary policy (e.g. uniform policy). In practice, we can directly use $w_\phi(s,a)$ to replace the original tactile danger potential $f_\varphi(s,a)$ in velocity modulation. The n-step tactile danger potentials with different $T$ are shown in Fig. 6a-6c. We see that the n-step tactile danger potential is just a smoothed version of the original potential. We collectively refer the tactile danger model in the strategy layer and the tactile danger potential in the modulation layer as tactile danger model (TDM), because they are almost equivalent when using neural networks. The difference in names comes from their different application scenarios.

### C. Tactile Defensiveness Layer

Animals have an innate ability to flee from dangerous contact events. Such events can be triggered by various tactile signals, such as mechanical contact, temperature, tactile perception, etc. We mimic this instinct through a model-free reactive behavior. This mechanism has higher priority than any planned motion, in order to prevent damage.

*1) Single Triggered Sensor:* For each sensor $i$, there is a local frame whose $z$ axis points outwards the body surface. The pose of sensor $i$'s frame is described by $r_i(t)$ in the world frame, and the corresponding Jacobian matrix

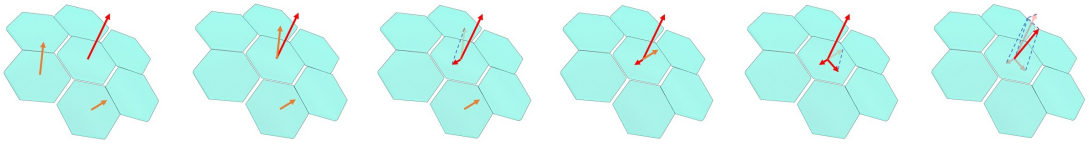

(a) (b) (c) (d) (e) (f)

Fig. 7: Merging multi-contact retraction trajectories. (a) retraction trajectories by different sensors, the red is the dominant trajectory; (b-c) the second trajectory is mapped to the dominant frame and projected to the null space of the dominant trajectory; (d-e) similar for the third trajectory, projected to the common null space of the dominant and the second trajectory; (f) the final trajectory is the sum of all projected trajectories.

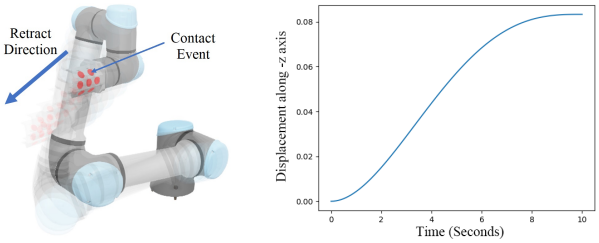


(a) (b)

Fig. 8: (a) Robot performing tactile defensiveness under contact; (b) displacement along -z axis of retraction trajectory.

is $\mathbf{J}_i(q)$. $q$ is the robot configuration, which can be a part of the robot state $s$. $\mathbf{J}_i(q) \in \mathbb{R}^{6\times n}$ if $r_i(t)$ is represented by xyz&Euler angles, and its size varies depending on the choice of its representation. $n$ is the number of joints. The relation between Cartesian velocity and joint space velocity is represented as:

$$\dot{r}_i(t) = \mathbf{J}_i(q) \cdot \dot{q}(t) \tag{9}$$

The tactile defensiveness behavior is triggered when sensor $i$ detects a tactile danger event defined in section III-A. We expect the retraction motion of sensor $i$ from its current pose to a safer pose along the opposite direction of the sensor normal (Fig. 8a). Assuming at time step $\tau$, sensor $i$ detected a danger event, its $z$ axis at $\tau$ is $z_i(\tau)$, and the Cartesian position is $p_i(\tau) \in \mathbb{R}^3$. The desired trajectory should follow:

- $\|p_i(\tau+T) - p_i(\tau)\| \propto \alpha \cdot f_i$
- $\dot{p}_i(\tau) = \dot{p}_i(\tau+T) = 0$

$\alpha$ and $T$ are hyperparameters. $\alpha$ is a sensitivity factor that controls how strongly the robot reacts to a danger event. $T$ is an agility factor that controls how long the retraction lasts. The first property shows that the retraction distance is proportional to the sensitivity factor and the severity of the danger event. This is consistent with animal behavior: retraction behavior is more responsive when the sensing system is more sensitive or when the contact force is high. The second property assumes the contact stops the robot immediately and the retraction motion will stop the robot at a safer position. An example trajectory function that fulfills the two properties is:

$$p_i(t) = -\alpha \cdot f_i \left( \frac{(t-\tau)^4}{4T^4} - \frac{2(t-\tau)^3}{3T^3} + \frac{(t-\tau)^2}{2T^2} \right) z_i(\tau) + p_i(\tau) \quad \tau \le t \le \tau + T \tag{10}$$

Such trajectory is first- and second-order differentiable (Fig. 8b). Thus, the desired spatial trajectory can be derived by setting its rotational velocity as zero, $\dot{r}_i(t) = [\dot{p}_i(t), 0]^T \in \mathbb{R}^6$. Then the joint space trajectory can be derived by:

$$\dot{q}_i(t) = \mathbf{J}_i^{-1}(q)\, \dot{r}_i(t) \tag{11}$$

Such trajectory can be tracked by a velocity controller.

*2) Multiple Triggered Sensors:* When multiple tactile sensors are triggered simultaneously, coordinating the composite behavior becomes especially important. Due to the limited number of robot degrees of freedom (DoFs), it is less possible to perform all the desired trajectories of the triggered sensors by Equation 11. Alternatively, the robot should retract from more severe tactile danger events first, and then from less severe ones. Thus, a priority based retraction coordinator should be devised.

In multi-contact setting, the time steps of danger events on different sensors are marked as $\tau_i$. Retraction is only performed in its active period $\tau_i \le t \le \tau_i + T$. We can build a pool containing all active sensors to control them centrally. First, all active sensors in the pool should be sorted by their emergent priorities. The priority $w_i(t)$ is defined as:

$$w_i(t) = \frac{\alpha \cdot f_i}{12} - [p_i(t) - p_i(\tau_i)]^T \cdot z_i(\tau_i) \tag{12}$$

The priority reduces from $\frac{\alpha \cdot f_i}{12}$ (maximum displacement of Equation 10) to 0 in the period of retraction. Then the triggered sensors are re-indexed by their priorities from high to low. The sensor with the highest priority is reindexed as $j = 0$ and its desired trajectory dominates. The idea is that lower-priority trajectories will affect higher-priority ones as little as possible. Also, as priority attenuates with time, a higher-priority trajectory may become lower-priority one later, and the index of a particular sensor may change.

Sensors have their own local frames. However, merging the trajectories of all active sensors can only be done in the same frame. We choose dominant sensor's frame as the reference frame and map the trajectories of other sensors from their local frames to the dominant frame. Assuming the number of the robot's DoFs is much smaller than the total number of tactile sensors, executing the trajectory of a particular sensor will inevitably affect the motion of other sensors. Here, null-space projection is adopted to ensure that executing lower-priority trajectories will cause minimum interference with higher-priority ones. The resultant joint velocity merging all active sensors is shown in Equation 13,

$$\dot{q} = \mathbf{J}_0^{-1} \left[ \dot{r}_0 + \sum_{j=0}^{j} \prod_{k=0} \left( \mathbf{I} - \varepsilon \cdot \bar{\dot{r}}_{k-0} \cdot \bar{\dot{r}}_{k-0}^T \right) \cdot \dot{r}_{(j+1)-0} \right] \quad \dot{r}_{i-0} = \mathbf{J}_0 \cdot \mathbf{J}_i^{-1} \cdot \dot{r}_i \quad \forall i \tag{13}$$

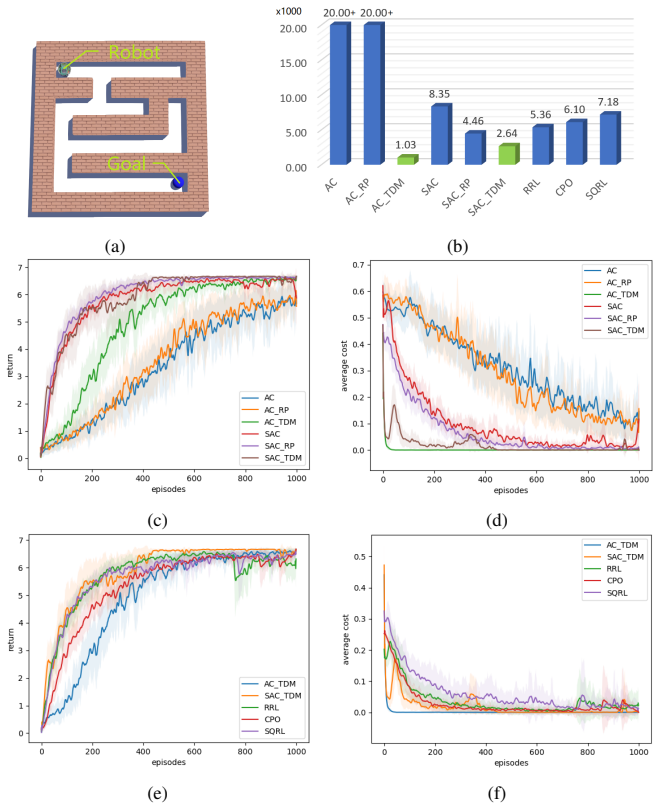


Fig. 9: Strategy layer results. (a) maze layout; (b) total contact events; (c) return curves and (d) cost curves of SAC and AC with different extensions; (e) return curves and (f) cost curves compared with safe RL baselines.

where $\bar{\dot{r}}_{k-0} = \dot{r}_{k-0}/\|\dot{r}_{k-0}\|$. $\varepsilon \in [0,1]$ is the tuning factor. When $\varepsilon \to 1$, the motion of sensor $j$ causes minimum interference with motion of sensors with higher priorities as full null-space projection. When $\varepsilon \to 0$, the total motion is simply the sum of trajectories of all sensors. The merging procedure is visualized in Fig. 7a.

## IV. EXPERIMENTS

In this section, we first conduct separate tasks to show the performance of the proposed three layers. We then show multiple layers are integrated to ensure safety in a teleoperated human-robot collaborative assembly task.

### A. Strategy Layer Performance

We tested the performance of the strategy layer with a reinforcement learning (RL) navigation task that requires repeated interaction with the environment to gather experience. We adopted a robot maze navigation scenario in Fig. 9a to show the strategy layer improves RL performance in terms of convergence speed as well as exploration safety. The robot navigates from the starting position to the goal position, minimizing the total contact with the maze walls. The state is the position of the robot in the maze. The action space contains 4 macro-actions: go forwards and backwards, turn left and right. Rewards are sparse: only +100 when the robot reaches the goal. Any collision will return a -1 cost. To show our approach is algorithm-agnostic, we implemented the strategy layer module to an off-policy

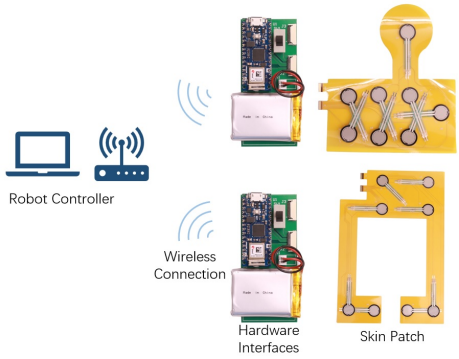


Fig. 10: Robot skin design.

algorithm, Soft Actor-Critic (SAC) [39] and an on-policy algorithm, Actor-Critic (AC) [40]. The return and cost curves are shown in Figs. 9c and 9d respectively. Baselines include (1) reward-penalty, the reward will be reduced by the cost (-RP suffix) [41], and (2) algorithms extended by our Tactile Danger Model (-TDM). We also compared several safe RL baselines, including recovery reinforcement learning (RRL) [42], constrained policy optimization (CPO) [43] and safe Q-functions for reinforcement learning (SQRL) [44]. The results are shown in Figs. 9e and 9f. From the cost curves in Figs. 9d and 9f, our "-TDM" mechanism shows the lowest total collision chance, which is also supported by the contact event statistics shown in Fig. 9b.

### B. Modulation Layer Performance

To demonstrate the effectiveness of the modulation layer, we ran an UR5 robot arm trajectory tracking experiment (Fig. 11a). Self/environment collision detection is turned on to precisely capture on-body collision locations to simulate full-body tactile sensors. Several solid balls are placed along the trajectory to generate collision. We compared the vanilla velocity controller trajectory tracking, velocity modulation by TDM, and velocity modulation with a 2-step TDM. The resultant trajectories of the three methods are shown in Fig. 11b-11d. From the figure we see that the vanilla velocity controller follows the trajectory correctly but causes large amount of collisions. Modulation by TDM can deviate from the trajectory and cause unintentional collisions. We assume that is because TDM learns sharp edges at the object boundary, and the robot's velocity can be modulated unpredictably. The n-step model learns a softer boundary, so the velocity is gradually penalized, resulting in smoother trajectories with fewer contacts. Since learning a good model requires repeated interaction with the environment, we reran this trajectory tracking task many times (episodes) and expect the performance to improve with more interaction experiences and better model quality. The quantitative result is shown in Fig. 11e. The non-modulated approach gets the highest collision chance. TDM modulation reduces contacts chance, but doesn't improve with more training. The 2-step TDM method almost reaches collision-free performance after 6 episodes. The sudden rising in episode 2 may attribute to that modulation repels the robot to unexplored areas, resulting new accidental collisions. These new experiences

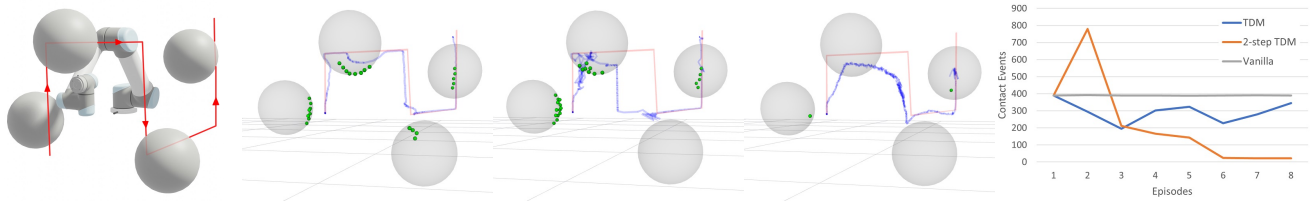


(a) (b) (c) (d) (e)

Fig. 11: Modulation layer results. (a) Desired end-effector trajectory; (b) trajectory (blue) of no modulation, green dots are contact points; (c) trajectory of TDM modulation; (d) trajectory of 2-step TDM modulation; (e) trend of the total number of contacts by episodes.

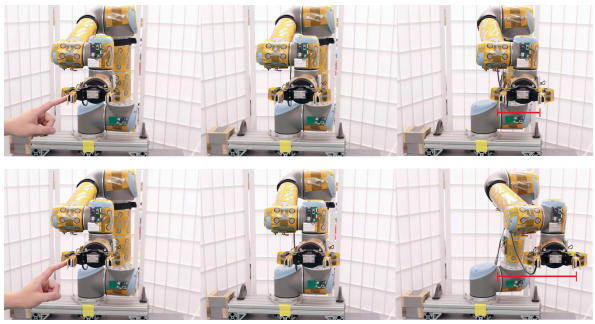

Fig. 12: (top) Retraction by light touch; (bottom) retraction by heavy touch. Red line shows the retraction distance.

will update the model and improve the performance in subsequent episodes.

### C. Robot Skin Design

We designed a modular robot skin as shown in Fig. 10. Each skin module consists of a flex-printed circuits (FPC) with Force Sensing Resistors array on it surface. The shape of FPC can customized to fit the local robot surface. A self-powered interface board digitalizes the recorded values on each sensor and transmits wirelessly to the robot controller. Such modular and flex-rigid separation non-invasive design simplifies the requirement of wiring and maintenance.

### D. Integrated Teleoperating System

Teleoperation, especially on the robot side, is highly vulnerable to accidental damage [45] due to poor sensory sharing or transmission delays [46] between the human and the robot. We designed an integrated teleoperating system by an UR5 robot arm with Robotiq 2f-85 Gripper synchronizing the motion of the human arm captured by our intelligent glove with VR tracker (Fig. 13). When an unexpected contact happens, the system enters the safeguarding mode governed by our tactile safety mechanisms. The retraction behavior under different force magnitudes are shown in Fig. 12. We see the robot is more responsive under heavier touch. Fig. 14 demonstrated the coordinated performance from different layers. When the robot is touched on the top, the tactile defensiveness layer generates retraction movement downwards. Under the regulation of the modulation layer, the robot stops before colliding with the desk.

We validated our proposed mechanism through a human-robot collaboration task. A human worker assembles an aluminum frame. Another UR5 robot assists the worker by delivering tools and frame parts. A demonstration is shown

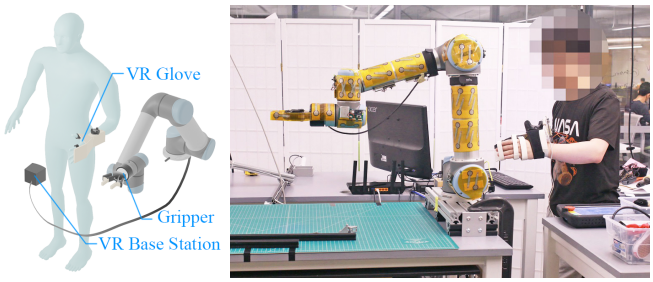


Fig. 13: Teleoperating system.

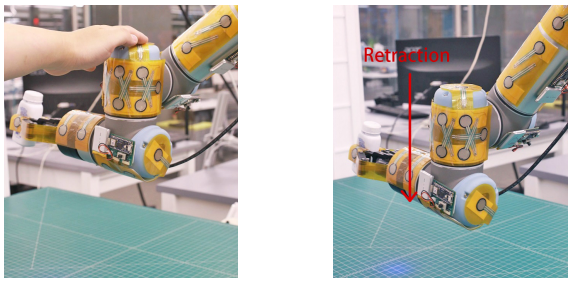


(a) (b)

Fig. 14: (a) External contact on the top of the robot; (b) the robot retracts towards the desk and stops before colliding with the desk under the regulation of modulation layer.

in Fig. 15. When the robot accidentally hits the human, it retracts to ensure the safety of the worker.

## V. CONCLUSION

In this paper, we comprehensively analyzed the robot tactile safety problem using full-body tactile sensors. We proposed a three-layer safeguard mechanism to address the problem hierarchically. A low-cost scalable modular robot skin was designed and implemented in our teleoperating system. We showed with a human-robot collaboration task that the proposed system performs safely when accidental collision happens.

(a) (b) (c)

Fig. 15: (a) The robot delivers parts when the human worker is doing the assembling task; (b) unexpected collision when the human worker fetches the part; (c) the robot retracts from the contact area.

## REFERENCES


[1] M. Lambeta, P.-W. Chou, S. Tian, B. Yang, B. Maloon, V. R. Most, D. Stroud, R. Santos, A. Byagowi, G. Kammerer, *et al.*, "Digit: A novel design for a low-cost compact high-resolution tactile sensor with application to in-hand manipulation," *IEEE Robotics and Automation Letters*, vol. 5, no. 3, pp. 3838–3845, 2020.

[2] K. Park, H. Park, H. Lee, S. Park, and J. Kim, "An ert-based robotic skin with sparsely distributed electrodes: Structure, fabrication, and dnn-based signal processing," in *2020 IEEE International Conference on Robotics and Automation (ICRA)*. IEEE, 2020, pp. 1617–1624.

[3] P. Ribeiro, S. Cardoso, A. Bernardino, and L. Jamone, "Highly sensitive bio-inspired sensor for fine surface exploration and characterization," in *2020 IEEE International Conference on Robotics and Automation (ICRA)*. IEEE, 2020, pp. 625–631.

[4] W. Yuan, S. Dong, and E. H. Adelson, "Gelsight: High-resolution robot tactile sensors for estimating geometry and force," *Sensors*, vol. 17, no. 12, p. 2762, 2017.

[5] G. Cheng, E. Dean-Leon, F. Bergner, J. R. G. Olvera, Q. Leboutet, and P. Mittendorfer, "A comprehensive realization of robot skin: Sensors, sensing, control, and applications," *Proceedings of the IEEE*, vol. 107, no. 10, pp. 2034–2051, 2019.

[6] N. Sommer and A. Billard, "Multi-contact haptic exploration and grasping with tactile sensors," *Robotics and autonomous systems*, vol. 85, pp. 48–61, 2016.

[7] M. Kaboli, R. Walker, G. Cheng, *et al.*, "In-hand object recognition via texture properties with robotic hands, artificial skin, and novel tactile descriptors," in *2015 IEEE-RAS 15th International Conference on Humanoid Robots (Humanoids)*. IEEE, 2015, pp. 1155–1160.

[8] K. Yao, M. Kaboli, and G. Cheng, "Tactile-based object center of mass exploration and discrimination," in *2017 IEEE-RAS 17th International Conference on Humanoid Robotics (Humanoids)*. IEEE, 2017, pp. 876–881.

[9] B. Sundaralingam and T. Hermans, "In-hand object-dynamics inference using tactile fingertips," *IEEE Transactions on Robotics*, 2021.

[10] P. Mittendorfer, E. Yoshida, T. Moulard, and G. Cheng, "A general tactile approach for grasping unknown objects with a humanoid robot," in *2013 IEEE/RSJ International Conference on Intelligent Robots and Systems*. IEEE, 2013, pp. 4747–4752.

[11] S. Christen, S. Stevšić, and O. Hilliges, "Guided deep reinforcement learning of control policies for dexterous human-robot interaction," in *2019 International Conference on Robotics and Automation (ICRA)*. IEEE, 2019, pp. 2161–2167.

[12] M. Koptev, N. Figueroa, and A. Billard, "Neural joint space implicit signed distance functions for reactive robot manipulator control," *IEEE Robotics and Automation Letters*, vol. 8, no. 2, pp. 480–487, 2022.

[13] H. Flor, "Painful memories," *EMBO reports*, vol. 3, no. 4, pp. 288–291, 2002.

[14] C. L. von Baeyer, T. A. Marche, E. M. Rocha, and K. Salmon, "Children's memory for pain: overview and implications for practice," *The journal of Pain*, vol. 5, no. 5, pp. 241–249, 2004.

[15] A. Gallace and C. Spence, "The cognitive and neural correlates of tactile memory." *Psychological bulletin*, vol. 135, no. 3, p. 380, 2009.

[16] H. Aonuma, "Serotonergic control in initiating defensive responses to unexpected tactile stimuli in the trap-jaw ant odontomachus kuroiwae," *Journal of Experimental Biology*, vol. 223, no. 19, 2020.

[17] C.-K. Song, J. Herberholz, and D. H. Edwards, "The effects of social experience on the behavioral response to unexpected touch in crayfish," *Journal of experimental biology*, vol. 209, no. 7, pp. 1355–1363, 2006.

[18] Y. Momohara, M. Yoshida, and T. Nagayama, "Serotonergic modulation of social status-dependent behavioural plasticity of the crayfish avoidance reaction," *Journal of Comparative Physiology A*, vol. 201, no. 11, pp. 1063–1074, 2015.

[19] L. Eidietis, "The tactile-stimulated startle response of tadpoles: acceleration performance and its relationship to the anatomy of wood frog (rana sylvatica), bullfrog (rana catesbeiana), and american toad (bufo americanus) tadpoles," *Journal of Experimental Zoology Part A: Comparative Experimental Biology*, vol. 305, no. 4, pp. 348–362, 2006.

[20] A. Kasumyan, "Tactile reception and behavior of fish," *Journal of Ichthyology*, vol. 51, no. 11, pp. 1035–1103, 2011.

[21] C. X. He, D. A. Cantu, S. S. Mantri, W. A. Zeiger, A. Goel, and C. Portera-Cailliau, "Tactile defensiveness and impaired adaptation of neuronal activity in the fmr1 knock-out mouse model of autism," *Journal of Neuroscience*, vol. 37, no. 27, pp. 6475–6487, 2017.

[22] C. F. Moore, L. L. Gajewski, N. K. Laughlin, M. L. Luck, J. A. Larson, and M. L. Schneider, "Developmental lead exposure induces tactile defensiveness in rhesus monkeys (macaca mulatta)," *Environmental Health Perspectives*, vol. 116, no. 10, pp. 1322–1326, 2008.

[23] J. L. Rhudy and C. R. France, "Defining the nociceptive flexion reflex (nfr) threshold in human participants: a comparison of different scoring criteria," *Pain*, vol. 128, no. 3, pp. 244–253, 2007.

[24] R. S. Dahiya, P. Mittendorfer, M. Valle, G. Cheng, and V. J. Lumelsky, "Directions toward effective utilization of tactile skin: A review," *IEEE Sensors Journal*, vol. 13, no. 11, pp. 4121–4138, 2013.

[25] J. Rogelio Guadarrama Olvera, E. D. Leon, F. Bergner, and G. Cheng, "Plantar tactile feedback for biped balance and locomotion on unknown terrain," *International Journal of Humanoid Robotics*, vol. 17, no. 01, p. 1950036, 2020.

[26] T. Kobayashi, E. Dean-Leon, J. R. Guadarrama-Olvera, F. Bergner, and G. Cheng, "Whole-body multicontact haptic human–humanoid interaction based on leader–follower switching: A robot dance of the "box step"," *Advanced Intelligent Systems*, vol. 4, no. 2, p. 2100038, 2022.

[27] J. Liang, J. Wu, H. Huang, W. Xu, B. Li, and F. Xi, "Soft sensitive skin for safety control of a nursing robot using proximity and tactile sensors," *IEEE Sensors Journal*, vol. 20, no. 7, pp. 3822–3830, 2019.

[28] A. Jain, M. D. Killpack, A. Edsinger, and C. C. Kemp, "Reaching in clutter with whole-arm tactile sensing," *The International Journal of Robotics Research*, vol. 32, no. 4, pp. 458–482, 2013.

[29] T. Pang, J. Umenberger, and R. Tedrake, "Identifying external contacts from joint torque measurements on serial robotic arms and its limitations," in *2021 IEEE International Conference on Robotics and Automation (ICRA)*. IEEE, 2021, pp. 6476–6482.

[30] A. Del Prete, F. Nori, G. Metta, and L. Natale, "Control of contact forces: The role of tactile feedback for contact localization," in *2012 IEEE/RSJ International Conference on Intelligent Robots and Systems*. IEEE, 2012, pp. 4048–4053.

[31] N. Kuppuswamy, A. Alspach, A. Uttamchandani, S. Creasey, T. Ikeda, and R. Tedrake, "Soft-bubble grippers for robust and perceptive manipulation," in *2020 IEEE/RSJ International Conference on Intelligent Robots and Systems (IROS)*. IEEE, 2020, pp. 9917–9924.

[32] Y. Zhang, G. Zhang, Y. Du, and M. Y. Wang, "Vtacarm. a vision-based tactile sensing augmented robotic arm with application to human-robot interaction," in *2020 IEEE 16th International Conference on Automation Science and Engineering (CASE)*. IEEE, 2020, pp. 35–42.

[33] A. Albini, F. Grella, P. Maiolino, and G. Cannata, "Exploiting distributed tactile sensors to drive a robot arm through obstacles," *IEEE Robotics and Automation Letters*, vol. 6, no. 3, pp. 4361–4368, 2021.

[34] M. Pfanne, M. Chalon, F. Stulp, H. Ritter, and A. Albu-Schäffer, "Object-level impedance control for dexterous in-hand manipulation," *IEEE Robotics and Automation Letters*, vol. 5, no. 2, pp. 2987–2994, 2020.

[35] Z. Ye, G. Pang, K. Xu, Z. Hou, H. Lv, Y. Shen, and G. Yang, "Soft robot skin with conformal adaptability for on-body tactile perception of collaborative robots," *IEEE Robotics and Automation Letters*, vol. 7, no. 2, pp. 5127–5134, 2022.

[36] T. Pang and R. Tedrake, "Easing reliance on collision-free planning with contact-aware control," in *2022 International Conference on Robotics and Automation (ICRA)*. IEEE, 2022, pp. 8375–8381.

[37] S. M. Khansari-Zadeh and A. Billard, "A dynamical system approach to realtime obstacle avoidance," *Autonomous Robots*, vol. 32, no. 4, pp. 433–454, 2012.

[38] L. Huber, J.-J. Slotine, and A. Billard, "Fast obstacle avoidance based on real-time sensing," *IEEE Robotics and Automation Letters*, vol. 8, no. 3, pp. 1375–1382, 2022.

[39] T. Haarnoja, A. Zhou, K. Hartikainen, G. Tucker, S. Ha, J. Tan, V. Kumar, H. Zhu, A. Gupta, P. Abbeel, *et al.*, "Soft actor-critic algorithms and applications," *arXiv preprint arXiv:1812.05905*, 2018.

[40] R. S. Sutton and A. G. Barto, *Reinforcement learning: An introduction*. MIT press, 2018.

[41] C. Tessler, D. J. Mankowitz, and S. Mannor, "Reward constrained policy optimization," *arXiv preprint arXiv:1805.11074*, 2018.

[42] B. Thananjeyan, A. Balakrishna, S. Nair, M. Luo, K. Srinivasan, M. Hwang, J. E. Gonzalez, J. Ibarz, C. Finn, and K. Goldberg, "Recovery rl: Safe reinforcement learning with learned recovery zones," *IEEE Robotics and Automation Letters*, vol. 6, no. 3, pp. 4915–4922, 2021.

[43] J. Achiam, D. Held, A. Tamar, and P. Abbeel, "Constrained policy optimization," in *International Conference on Machine Learning*. PMLR, 2017, pp. 22–31.

[44] K. Srinivasan, B. Eysenbach, S. Ha, J. Tan, and C. Finn, "Learning to be safe: Deep rl with a safety critic," *arXiv preprint arXiv:2010.14603*, 2020.

[45] J. A. Fishel, T. Oliver, M. Eichermueller, G. Barbieri, E. Fowler, T. Hartikainen, L. Moss, and R. Walker, "Tactile telerobots for dull, dirty, dangerous, and inaccessible tasks," in *2020 IEEE International conference on robotics and automation (ICRA)*. IEEE, 2020, pp. 11 305–11 310.

[46] M. Franken, S. Stramigioli, S. Misra, C. Secchi, and A. Macchelli, "Bilateral telemanipulation with time delays: A two-layer approach combining passivity and transparency," *IEEE transactions on robotics*, vol. 27, no. 4, pp. 741–756, 2011.